

## **GEOMECHANICS FOR HYDROCARBON PRODUCTION: ON THE IMPLEMENTATION OF PULSED ARC ELECTRICAL DISCHARGES FOR STIMULATION PURPOSES**

Gilles Pijaudier-Cabot<sup>1</sup>, Christian La Borderie<sup>2</sup>, Youssef Fawaz<sup>1,2</sup>, Pascale Sénéchal<sup>3</sup>, Antoine Jacques<sup>4</sup>

<sup>1</sup>E2S UPPA, Laboratoire des Fluides Complexes et leurs Réservoirs, UMR 5150, Université de Pau et des Pays de l'Adour/CNRS/Total, Anglet, France

<sup>2</sup>E2S UPPA, SIAME, Université de Pau et des Pays de l'Adour, Anglet, France

<sup>3</sup>E2S UPPA, DMEX Center for X-ray Imaging, UMS 3360, Université de Pau et des Pays de l'Adour/CNRS, Pau, France

<sup>4</sup>TOTAL E&P, CSTJF, Avenue Larribau, Pau, France

Keywords: Hydraulic Fracturing, Dynamic Stimulation, Shock wave, Clogging-unclogging of fracture, Permeability

### **ABSTRACT**

This contribution addresses the implementation of Pulsed Arc Electrohydraulic Discharges (PAED) techniques in geomechanics with two objectives: first the development of an alternative to classical hydraulic fracturing, and second the stimulation of existing fracture aimed at increasing the production of oil or gas. Experiments reproducing PAED and the induced fracture in rocks under reservoir conditions are first described. The influences of the amplitude of the shock wave and of the number of shocks applied to laboratory specimens on damage and on the intrinsic permeability of the material are illustrated. Then, a computational model that simulates the entire process is discussed. As far as the stimulation of existing fractures is concerned, the issue is to flush out the various particles that may be packed within the propped fracture and may induce a decrease of permeability of the fracture viewed as a drain for hydrocarbon production. The shock wave generated inside the borehole by PAED is converted into surface waves travelling on the fracture surface. These waves induce fast variations of pressure in the fracture that may potentially destabilize flocculates and put in suspension particles. Experiments illustrate the clogging-unclogging effects as a function of the density of fine that are introduced in order to promote clogging. These results should further help at understanding the basic parameters that govern the clogging-unclogging processes and therefore understanding what could be the best conditions of applicability of the PAED unclogging technique.

### **INTRODUCTION**

Shock waves generated in water by Pulsed Arc Electrohydraulic Discharges (PAED) have offered over the past years new perspectives for the stimulation of hydrocarbon reservoirs aimed at increasing their production. Two specific issues shall be considered in the present contribution:

- First PAED techniques are investigated for the purpose of devising an alternative to hydraulic fracturing, which has a poor efficiency in non-conventional hydrocarbon production. PAED in boreholes generate a dynamic loading, a pressure wave that propagates in the rock formation. It generates fracture in a much more efficient way: because there is a

large amount of elastic energy transferred in the rock, a dense fracture network is induced. As the loading wave spreads inside the material, it will therefore create fragmentations, thereby connecting the initial and newly created network of cracks. Dense micro-cracking increases the rock permeability.

- The second application of PAED techniques deals with the restoration of the production of existing wells that have been fractured in the past. During service, fluids and gases flow cause particles to circulate in the fractures. These particles can adhere to the crack and grain surfaces and form clusters that may decrease drastically the permeability of the drains created by hydraulic fracturing. The pressure wave generated by PAED, may be used to destabilize these clusters and therefore to recover the initial drain permeability.

The major results obtained concerning these two issues are presented in the following, with a focus on experiments that have been devised in order to demonstrate the feasibility of PAED stimulation techniques.

## **ELECTRO-HYDRAULIC FRACTURING**

The following summarizes an experimental program carried out between years 2009 and 2013. A complete presentation of the results can be found in Refs [1-5]. The experimental program included several distinct phases: (i) mechanical experiments in which specimens were subjected to representative confinement stresses and to pulsed arc electro-hydraulic discharges, (ii) permeability tests performed before and after the mechanical experiments in order to quantify the increase of permeability upon electro-hydraulic fracturing, and (iii) X-ray scanning tomography before and after the mechanical experiments in order to visualize the crack network generated by the mechanical loads.

### **Mechanical set-up**

Our purpose was to design experiments that implement conditions as close as possible to real ones. It means that specimens ought to be subjected to the triaxial confinement experienced underground at several different depths, and that the applied pulse should be generated in a specimen geometry that is close to a real well bore.

The specimens are hollow cylinders with internal diameter, external diameter and height equal to 50 mm, 125 mm, and 180 mm respectively. Two materials have been considered: mortar and sandstone. The shock wave was generated inside the hollow cylinder filled with water. A radial confinement pressure was applied with three stacked steel rings (600 mm diameter, 60 mm height and 30 mm thick) tightened with the help of a beam wrench. The steel rings were equipped with strain gauges to check the confining pressure during the tightening phase. Three confining blocks made of ultra high performance fibre reinforced concrete were placed between the specimen and the steel rings in order to absorb the shock wave and to homogenize the radial pressure on the external face of the specimen. The high performance concrete used for confining the specimen has approximately the same dynamic impedance characteristics than the specimen in order to avoid wave reflections at the boundary. This set-up is illustrated in Fig. 1.

The vertical load was applied with a 2000kN hydraulic jack, which was placed in an protected environment with respect to electromagnetic radiations and electrical surges. Due to the radiations generated by the electrical discharges, it was possible to use neither LVDT transducers nor electronic equipment for load control or resistive gauge measurements. Hence, the frame was a pneumatic one, the confinement was applied in a passive way and no transducers could be placed in order to record loads or deformations.

Specimens have been confined according to three levels of radial stresses and vertical loads corresponding to three depths: low confinement (depth = 0 m), medium confinement (depth equal to 1500m and Biot factor equal to 1) and high confinement (depth equal to 2250 m and Biot factor equal to 0.5 or depth equal to 3000m and Biot factor equal to 1).

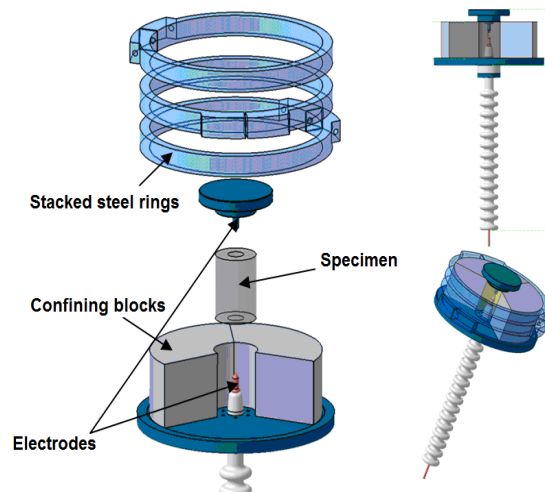


Figure 1 - Overall view of the triaxial cell.

The electrodes were placed inside the hollow part of the specimen immersed by water. The electrodes were made of two vertical cylindrical tubes on the lower ends of which were screwed two stainless steel electrodes (5 mm diameter). The gap between the two electrodes was 5 mm. The positive impulse voltage was obtained by charging storage capacitors in the range from  $C=300\text{nF}$  to  $21\mu\text{F}$ , depending on the electrical energy to be released during the electric discharge. A triggered spark-gap allowed the switching of energy of up to 20 kJ into water. The maximum charging voltage of the capacitors was 40kV. The voltage impulse and the current were monitored with a North Star probe (100kV-90MHz) and a Pearson current monitor (50kA-4MHz) respectively. According to previous investigations [6], the dynamic pressures generated by subsonic water discharges present bi-exponential form and are characterized by a rise time of about 500ns and a pulse width of a few microseconds. The associated frequency spectrum reaches 200 kHz at -20dB.

Radial permeability tests were performed in isothermal (ambient) conditions. An inert gas (nitrogen) is injected into the cylindrical borehole through a perforated bottom platen and flowed radially through the specimen. The relative pressure and mass flow rate were measured upstream to the specimen with a set of mass flow meters that converted the mass flow rate to an equivalent volumetric gas flow rate. Each flow meter had a different range, starting from 10–150 ml/min, 50–1500 ml/min, to 300–15000 ml/min, in order to adapt measurements to the increase of permeability.

In order to obtain the intrinsic permeability related to viscous laminar flow, a characteristic of the sole porous medium, the relationship due to Klinkenberg has been used [7]. The intrinsic permeability  $K$  [ $\text{m}^2$ ] is obtained by extrapolating the apparent gas permeability measured at various pressures to the case of infinite pressure. The measurements of the apparent permeability were performed for five relative pressures: 0.3, 0.25, 0.20, 0.15, and 0.10 MPa. The accuracy of measurement of the apparent permeability was 2% approximately. The permeability has been measured on each specimen prior to mechanical testing and served as a reference for further in comparisons.

Each specimen was scanned in a X-ray tomography facility at Total E&P laboratories prior and after testing. The specimens were marked so that the 3D images could be superimposed and then relative permanent displacements between the two images could be recovered. These residual displacements are assumed to be due to cracks that stay open after testing. The technique is such that residual crack opening of a few tenth of microns could be obtained from images with an accuracy of 250 micrometers corresponding to a medical X-ray tomographic device.

## Experimental results

Two sequences of tests have been carried out. In the first one, the specimens were subjected to a single shock under a variable injected electrical energy, for each of the three confinement levels considered. For the tests under low confinement, the injected electrical energy ranges up to 680J; for the tests under medium confinement, it ranged up to 1.15kJ and the injected energy reached 17kJ in the tests under high confinement. In a second type of test, the specimens were subjected to repeated shocks (up to 9 shocks) with a constant injected energy, respectively equal to 2.7kJ and 2.2kJ respectively. Note that the time between each shock is of the order of several minutes in order to avoid any possible fatigue effects.

Figure 2 shows the evolution of permeability observed for a single applied shock and for a series of low energy shocks under high confinement.

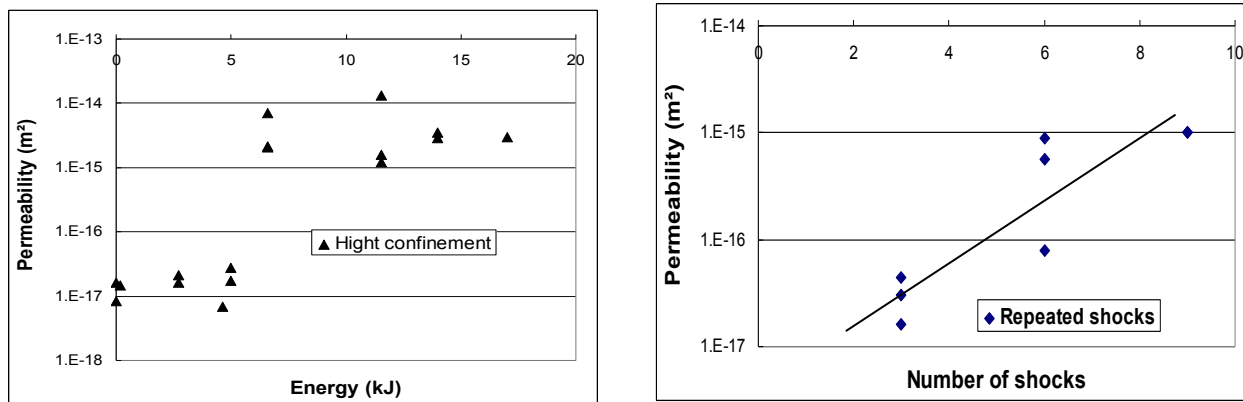


Figure 2 - Evolution of the permeability with injected electrical energy for a single shock on mortar specimens (left), and for repeated shocks (right). Tests under high confinement.

Under all confinement levels, if the injected electrical energy is below a threshold, the intrinsic permeability does not increase. This threshold increases with confinement. Then, permeability sharply increases with the injected energy. Repeated shocks have been applied at an energy level is 85 % of the threshold of damage. The number of shocks applied on each specimen ranged from 3, to 6 and 9 shocks. The test results are plotted in Fig. 2. in a semi-log plot, the permeability increases almost linearly with the number of shocks. This increase spans over a range of almost two orders of magnitude, which is above the scattering of data.

The correlations between the dynamic load applied on the specimens, their microstructure, material damage, and the permeability can be visualized qualitatively with X-ray tomography. Figure 3 shows the effect of the number of repeated shocks with injected electrical energy equal to 2.7kJ on the generation of macro-cracks under high confinement. After 3 shocks, cracking slightly evolves with a crack surface equal to 26 cm². Macro cracking occurs inside the specimen after 6 shocks and the crack surface increases to 238.5cm². After 9 shocks, severe cracking is observed and the crack surface is 326.5 cm².

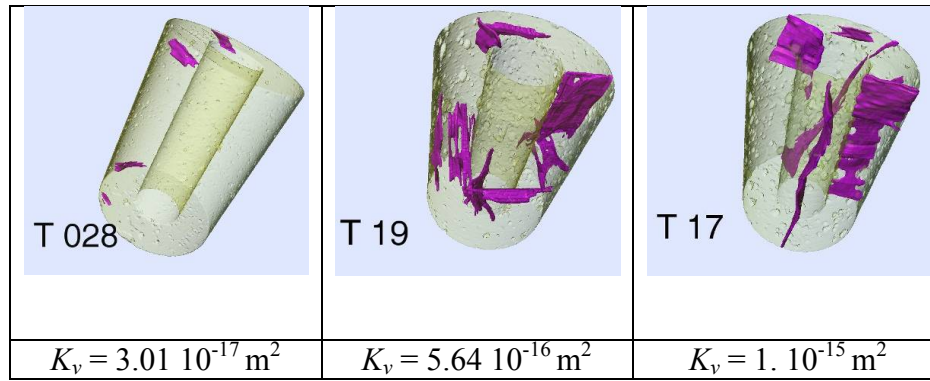


Figure 3 - 3D tomography scans after one shock (left), three shocks (middle) and nine shocks (right). Tests under high confinement.

### Computational modeling

Three items have been considered for a proper modelling of electro-hydraulic fracturing: (i) the theoretical model from which the pressure generated by the pulsed arc electric discharge can be derived, (ii) the mechanical modelling of the material under dynamic loads, and (iii) the coupled effects between the growth of damage due to micro-fracturing and the growth of permeability.

The simulation of shock wave generation in water by electrical discharges has been the subject of several studies over the recent years, in the context of the safety of sodium-water nuclear reactors. For instance, S. Madhavan and co-workers [8] performed one-dimensional and two-dimensional hydrodynamic simulations for studying shock production in water [4]. Here, a simplified model has been developed, capable to provide a correct characterisation of shock wave propagation in water. The hydrodynamic pressure wave results from the rapid injection of energy into water, as an augmentation of enthalpy. High-pressure bubbles are formed and expand very quickly. This motion of the boundaries between the liquid and the gas phase at high velocity generates the wave. The underwater electrical discharge is assumed to occur within a two-phase mixture, liquid water and water vapour, each phase being in thermodynamic equilibrium. The electrical discharge is represented by a time dependent insertion of energy in a small region located in between the electrodes. Once the pressure wave is generated (due to phase changes), it travels into water, reaches the solid specimen eventually, and then it is converted into an elastic wave that travels further in the solid phase.

Among many constitutive models for concrete and geomaterials (soils and rocks) devised in the literature, we have chosen to implement here a continuum damage-based model for several reasons: the first one is the simplicity of the constitutive relations, both from a theoretical point of view, but also from a computational point of view. The non-linear response of the material is controlled by a small set of parameters, computed directly as a function of the applied strains. Hence, the finite element implementation is explicit, which fits quite well with the overall computational scheme. A second reason for this choice is that the relationship between material damage (micro-cracking) and intrinsic permeability has some theoretical motivation [9], whereas relationships between strain and permeability do not, except in the case of Poiseuille flow in fully developed macro-cracks (see e.g. Refs. [10-12]), which is only the final stage of cracking considered here.

The constitutive relations used here are an extension of Desmorat's model [13], fulfilling the conservation of fracture energy upon quasi-static failure. This is required in order to cope with the difficulties coming from the strain softening response of the material [14]. The rate dependent damage model implemented here ensures well posedness of initial value problems in

the presence of strain softening but it does not prevent convergence towards zero energy dissipation upon failure [3]. Rate dependency is meant here to describe the increase of material strength with the strain rate in the absence of localisation of damage, whereas the energy dissipated upon fracture (corresponding to a completely damaged material) is set independently from the finite element size, same as in quasi-static fracture propagation.

A relationship between isotropic damage and the intrinsic permeability has been proposed by Bary and co-workers [15] and has been used also by Schreffler and co-workers [16] and Jason [17]. The formulae implemented by Jason in the context of isotropic (scalar) damage read:

$$K = K_0 \text{ if } D < D_0 \text{ and } K = K_0 \cdot 10^{c(D-D_0)} \text{ if } D \geq D_0 \quad (1)$$

with  $K_0$  the intrinsic permeability of undamaged material,  $K$  the intrinsic permeability of damaged material,  $D_0$  the damage threshold under which permeability is not affected by damage and  $D$  the damage scalar in an isotropic model.  $c$  is a model parameter. In the present case, damage is represented by a second-order tensor. We use the same type of relationship between damage and intrinsic permeability and directional effects on the permeability are inserted. The intrinsic permeability is a second order tensor and we assume that the principal directions of the damage tensor and of the permeability tensor coincide. Damage growth in one direction generates an increase of permeability in the two orthogonal directions. In other words, the augmentation of the permeability in one direction depends on the two perpendicular principal values of damage. Following this principle, permeability in direction  $i$  is computed according to the maximum value of damage in the two orthogonal directions  $(j,k)$ . Eq. (1) is adapted the anisotropic case accordingly:

$$\begin{aligned} K_i &= K_0 \text{ if } \text{Max}(D_j, D_k) \leq D_0 \\ K_i &= K_0 \cdot 10^{c(\text{Max}(D_j, D_k) - D_0)} \text{ if } \text{Max}(D_j, D_k) > D_0 \end{aligned} \quad (2)$$

where  $K_i$  is the permeability in the principal damage direction  $i$ .  $D_j$  and  $D_k$  are the values of damage in principal axes normal to axis  $i$ . Note that for the sake of simplicity, and in order to avoid additional calibration, the parameters ( $c=8.65$ ) and ( $D_0=0.035$ ) are kept the same as those fitted by Jason and co-workers.

These models have been folded into a single computer code, EUROPLEXUS co-developed by CEA (CEN Saclay, DMT) and the European Commission (JRC-Ispra, ISIS) since 1999. This code is based on the Finite Element Method and uses an explicit time integration algorithm [18-20]. At each time step, the conservation of mass, the conservation of energy, the constitutive laws, and the conservation of momentum are computed successively. The entire set-up (fluid and solid) is modelled with a single finite element mesh and an Arbitrary Lagrangien Eulerian (ALE) description is implemented in order to achieve a proper description of the fluid-solid interface [21].

Let us illustrate the capabilities of the computational model on the presented above. The geometry of the 3D finite element model and the boundary conditions are depicted in Fig. 4. It represents the entire mechanical set-up: the specimen filled with water and the high performance concrete blocks.

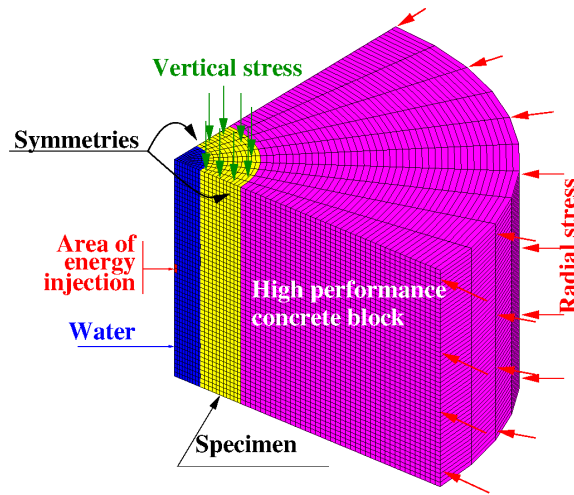


Figure 4 - Finite element model of the simulation of tests on hollow cylinders.

The evolution of the average permeability with injected energy is illustrated in Fig. 5. Note that this is not a fit. The model parameters have been calibrated on separate experiments without confining stresses. Therefore, the agreement between the model response and the experiments is a representative of the efficiency of the computational approach.

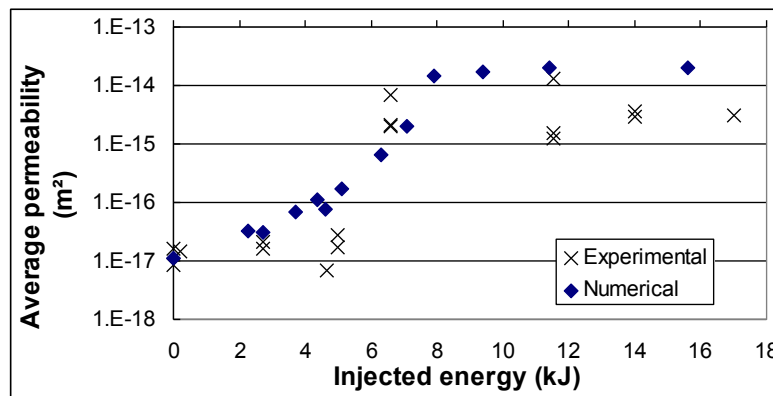


Figure 5 - Comparison of the experimental and the numerical average permeability under high confinement with variable injected energy.

In Ref. [5], full-scale simulations are also presented, along with several optimization routes in order to enhance the efficiency of the electro-hydraulic fracturing technique. Indeed, it is found that the stimulation method induces micro-cracking in the close neighborhood of the well-bore, mainly because the pressure wave is spherical and attenuates quite rapidly. Optimizations are expected to increase the size of the stimulated rock volume by a factor 5 to 10.

### CLOGGING-UNCLOGGING EXPERIMENTS

During well service, fluids and gases cause fine particles in the fractures that are generated by the hydraulic fracturing. These particles can clog the cracks resulting in a loss of well productivity. In order to understand better this process of fracture clogging and to remedy the issue of the productivity lack due to these sediments using PAED, we provide more detailed information in this section about an experimental apparatus developed recently to measure the permeability of clean, clogged and unclogged propped fracture using alternatively water and Nitrogen gas and to simulate the clogging and unclogging processes under dynamic loads.

**Experimental set-up**

To mimic the fracture, two Polycarbonate cylindrical samples were used with 46 mm in diameter and 50 mm in length (Fig. 6). Only the bottom sample has a 6mm borehole where fluid is injected and then flows in the space left between the two polycarbonate samples. This space which mimics the fracture is filled with proppant. A fixing system is provided on each sample on the edge to install later on 4 Nylon threaded rods (M6, D=6mm) with 8 nuts (4 from each side).

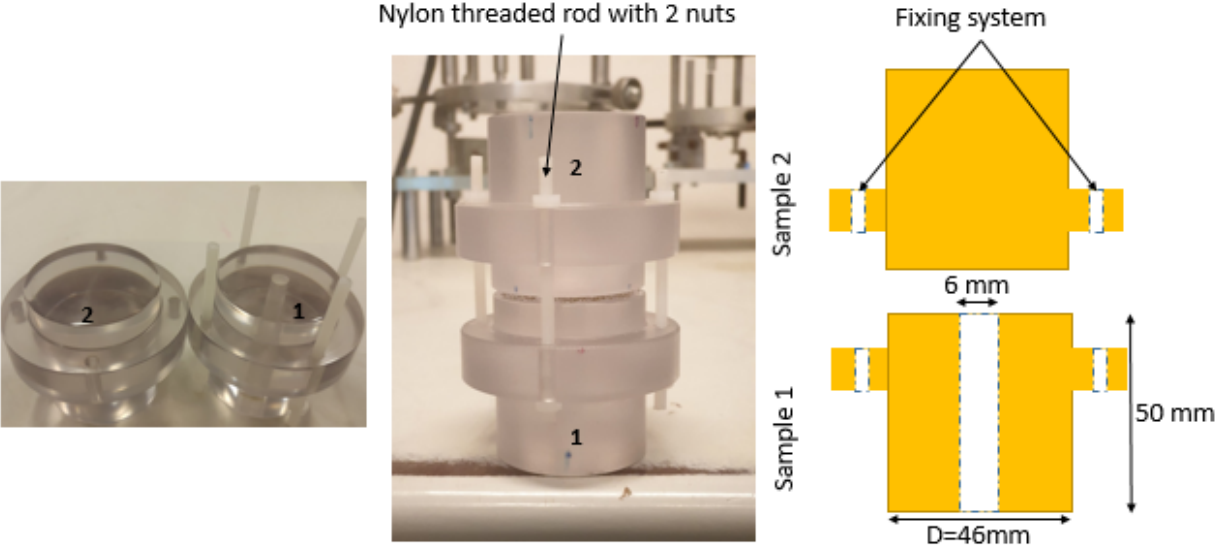


Figure 6- Polycarbonate samples details.

Polycarbonate material was chosen due to transparency, so that we may observe inside the fracture. Furthermore, this material is also almost transparent to X-rays.

Moving to the proppant, i.e. the granular skeleton inside the fracture, we used ceramic proppant mesh 40/70 with a median diameter of 315  $\mu\text{m}$  ( $212 \mu\text{m} < d < 425 \mu\text{m}$ ). The amount of proppant placed in the fracture is measured according to the density of proppant. Placed into a single layer on the crack surface, the density of proppant is 380-400  $\text{g}/\text{m}^2$ . Hence, for instance,  $\frac{1}{2}$  layer corresponds to a density of 190-200  $\text{g}/\text{m}^2$ . Figure 7 shows 2 pictures with a side view of a fracture filled with 2 layers of proppant mesh 40/70 and a fracture filled by 0.5 layer.

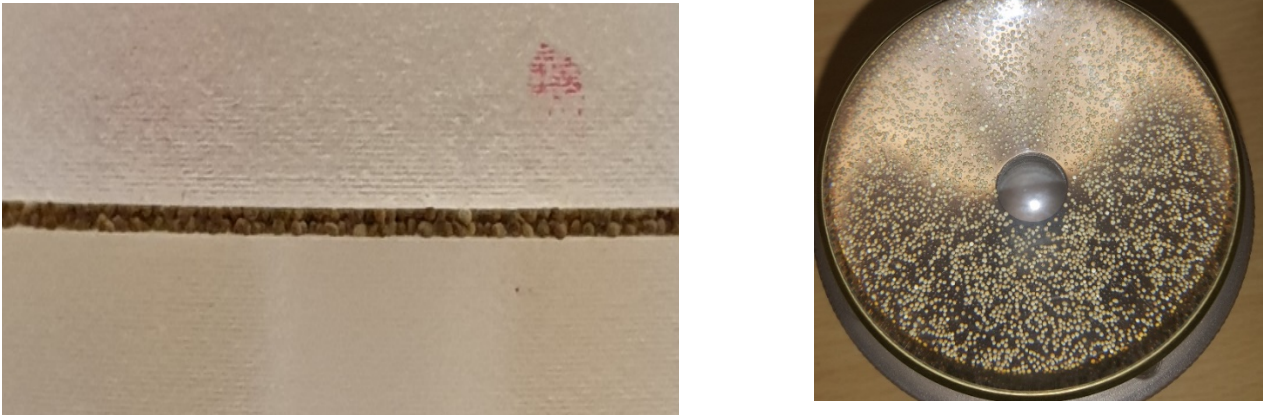


Figure 7- Left: Side view of a fracture filled with 2 layers of proppant; right: top view of a fracture filled with 0.5 layer.

As for the clogging materials, there are many sources of sediments and fine particles flowing inside the hydraulic fractures during the well service, like the creep matrix collapse, chemical reactions between fluids and fluids and solids (yielding precipitation of a solid phase), and proppant crushing. Here, we decided to clog the fractures with crushed natural sands ranging between 25 to 75  $\mu\text{m}$  in diameter.

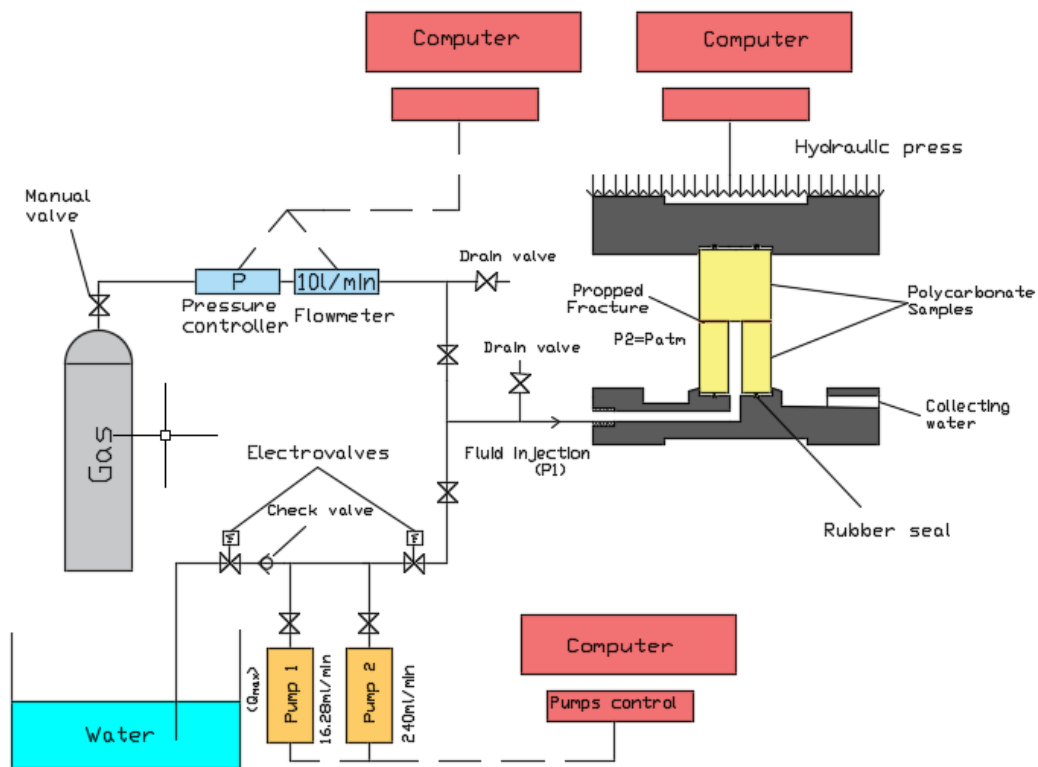


Figure 8- Schematic of the complete experimental apparatus.

The experimental set-up depicted in Fig. 8 has been designed to measure the permeability of the propped fracture under static and dynamic load. Two different circuits have been used to insure properly all the measurements. The gas circuit is dedicated to the measure of the gas permeability of the fracture using Nitrogen gas  $\text{N}_2$  with a high purity of 99%. This circuit includes a mass flow meter and a pressure controller. These two instruments are equipped with a pc-board, which contains all the general functions needed for measurement and control. A water circuit measures the permeability to liquid. It is made up of two pumps controlled by a computer. The first pump is dedicated to the measure of the water permeability, with a capacity of 16.28 ml/min. The second pump is used mainly to wash the fracture before starting the measurement of gas permeability (clean fracture without clogging) and during the unclogging process while applying the dynamic loads.

The hydraulic uniaxial frame Zwick Roell HB250 applies static and dynamic uniaxial loads on the polycarbonate specimen containing the fracture. To be close to the geological constraints, permeability measurements are performed under a static vertical stress of 20 MPa (Load= 34 kN). The dynamic loads (unclogging phase) are handled by the electro-valve offering the highest hydraulic flow rate (64 l/min) with different types of dynamic signal (sinusoidal, square....).

The experimental program follows 3 steps:

1. Measure the gas-water permeability of a clean fracture under a stress of 20 MPa: before setting up the sample under the hydraulic press, the proppant weight is determined

depending on the number of layers placed in. A natural soluble paste is spread on the top of the cylinder to stick proppant grains in order to have a uniform distribution. After installing the fracture, a washing phase with two water injections is done in order to clean out the paste before starting the gas-water permeability measurements.

2. Clog the fracture with crushed sand then measure the gas-water permeability: after placing the proppant, the fracture is clogged by distributing manually fine sands on the surface of the fracture (after the specimen has been opened). Once the sample is set up under the hydraulic press, two water injections are performed to let the fine particles take their place in the fracture before permeability measurements. After that, the fracture is scanned.
3. Unclogging process: application of dynamic uniaxial loads while injecting water with a constant flow rate followed by a permeability measurement and an x-ray scan. The measurement and treatment conditions of the clogged fractures in our experimental set-up are closely related to the operational conditions by generating dynamic waves in the fractures with continuous injection of water with a constant flow rate (240ml/min) into the well (borehole in the bottom cylinder). Water has a very important role to play in transporting fine particles to flush them away from the well. In addition, the generation of shock waves in water induces fluid pressure which may destabilize these aggregates adhered to the granular skeleton of the fracture and consequently proceed to the fracture cleaning. Square and sinusoidal signals were used with an amplitude of 9kN (5.4 MPa) and many frequencies: 1, 5, 10 Hz.

## Preliminary results

We present some typical results of 2 scanned fractures packed with different proppant densities (0.5 layer and 2 layers) and clogged with 15 % of fine sand.

First, a fracture with 0.5 layer was tested with a proppant density of 200 g/m<sup>2</sup>. The gas permeability of this fracture was 141.71 Da (clean fracture) measured under a stress of 20 MPa. It was clogged with 15% of fine sand. A significant decrease (65%) of the gas permeability was detected (49.4 Da).

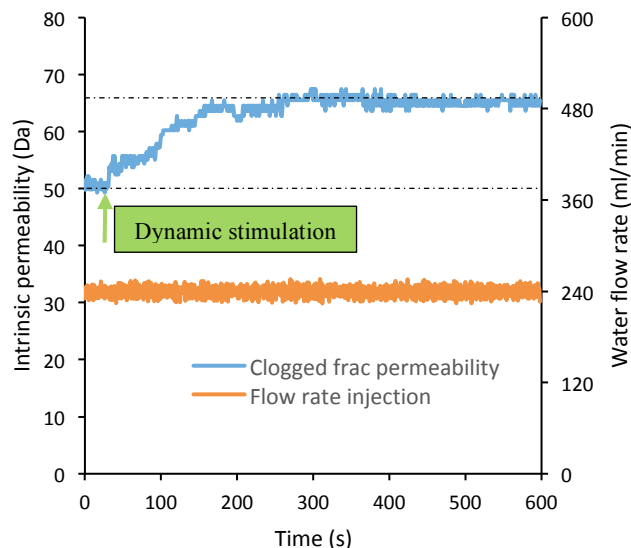


Figure 9- Permeability evolution after applying a dynamic load on a clogged fracture with 0.5 layer of proppant.

Figure 9 shows as the evolution of the intrinsic permeability with a constant water flow rate in the clogged fracture. A significant increase of the permeability is detected while applying a dynamic stimulation with a frequency of 10 Hz and an amplitude of 9kN (5.4 MPa). This is related to the fluid pressure wave generated due to the dynamic signal inside the fracture that destabilizes the clusters of fine sand and drag them out of the fracture through the injected fluid.

A fracture with 2 layers was tested with a proppant density of 800 g/m<sup>2</sup>. The gas permeability of this fracture was 56 Da measured under a stress of 20 MPa. It was clogged with 15% of fine sand. A significant decrease (80%) of the gas permeability was detected (11 Da).

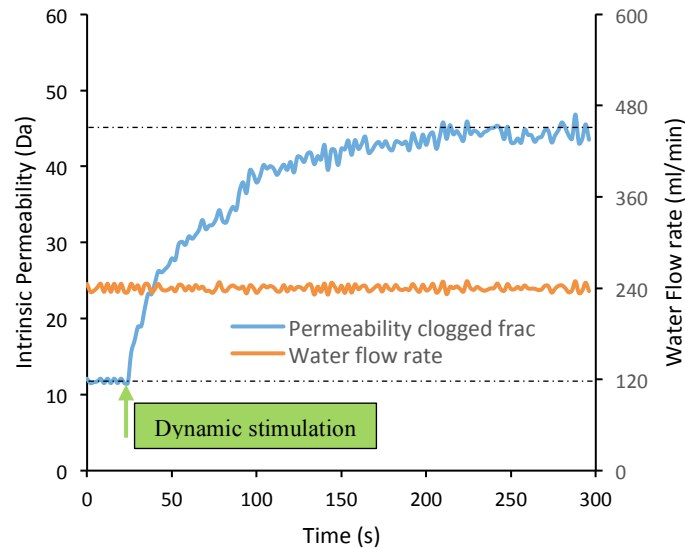


Figure 10- Permeability evolution after applying a dynamic load on a clogged fracture with 2 proppant layers.

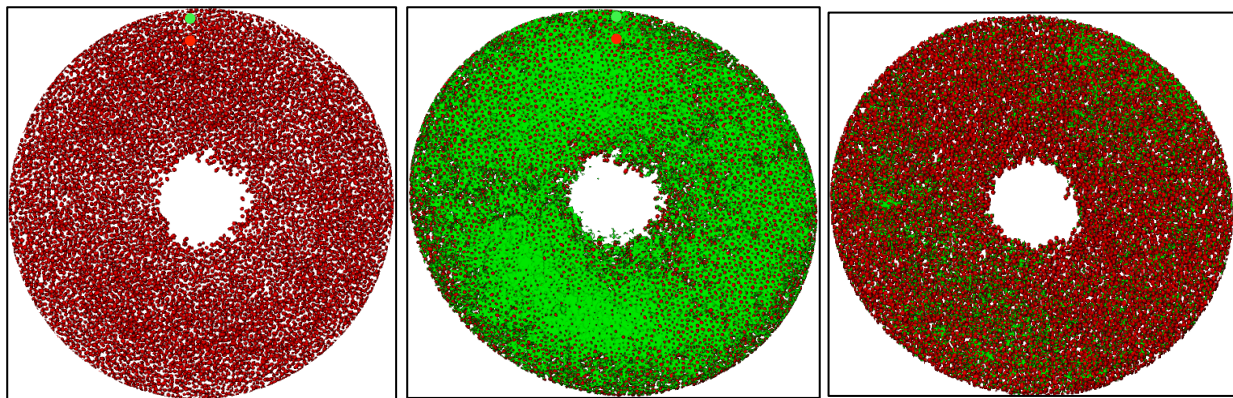


Figure 11- Xray images for scanned fractures at 18µm resolution: clean fracture (left), clogged fracture (middle), unclogged fracture (right). Particles in red are proppant particles, particles in green are crushed sand particles.

After clogging the fracture and measuring the intrinsic permeability under a stress of 20 MPa, we performed the unclogging process. Figure 10 shows the evolution of the intrinsic permeability with a constant injection of water flow rate (240 ml/min). A significant and sudden increase of the intrinsic permeability is noticed after applying the dynamic stimulation with a frequency of 10 Hz and an amplitude of 11 kN (6.7 MPa). The dynamic signal used was a square signal. The permeability reached after the stimulation is 45 Da, which corresponds to a recovery percentage of 75%.

We observe clearly in Fig. 11 that the fracture is almost cleaned after applying dynamic stimulation. The percentage of fines lost and migrated out of the measurement area (scanned) was 82%.

## CLOSURE

We have illustrated in this paper some of the potentialities of PAED techniques for enhancing hydrocarbon production:

PAED can be used for the purpose of creating a dense number of micro-cracks in rock formations aimed at enhancing their permeability. An increase of two to three orders of magnitude is observed in laboratory experiments. Computational simulations involve the modeling of the entire process, from the generation of the shock wave due to electrical discharge in water to the induced micro-cracks and the inherent increase of material permeability. It provides also a tool to extrapolate results to candidate rock formations. Such simulations demonstrated that the stimulated rock volume remains, however, quite restricted to the near well-bore region [5]. Optimization of the process has been also considered and, with an increase of the electrical energy that can be used for PAED (a few MJ) along with a conversion of the pressure wave from spherical to a plane wave, it should be possible to enlarge this volume substantially in order to reach realistic applications.

PAED can be also used at low energy levels for the purpose of cleaning existing fracture. Compared to electro-hydraulic fracturing, the mechanism involved is quite different: the pressure wave that is generated is converted into a surface wave propagating on the crack surface (hence is it much less attenuated). This surface wave generates variations of pressure inside the propped fracture that may destabilize flocculates that are formed during hydrocarbon production. A new experimental set-up has been presented for the purpose of understanding, and later on optimizing unclogging. In these experiments, the pressure wave is mimicked by a dynamic load applied on the fracture after it has been clogged. Preliminary results show that when the dynamic load is applied, the permeability of the fracture is increased with a recovery percentage that can be as high as 75%. Further works are expected to understand and simulate this unclogging process and to optimize the technique with the implementation of PAED instead of synthetic dynamic loads.

## ACKNOWLEDGEMENTS

Financial support from Total E&P is gratefully acknowledged. The authors would like to thank Dr. W. Chen, Dr. T. Reess, Dr. O. Maurel, Dr. A. de Ferron and Dr. F. Rey-Bethbeder who actively participated in the research on electro-hydraulic fracturing. X-Ray scans on clogging-unclogging experiments have been provided by E2S UPPA - DMEX center for X-ray Imaging.

## REFERENCES

- [1] Maurel, O., Reess, T., Matallah, M., De Ferron, A., Chen, W., La Borderie, C., Pijaudier-Cabot, G., Jacques, A., Rey-Bethbeder, F., Electrohydraulic shock wave generation as a mean to increase intrinsic permeability of mortar. In *Cement and Concrete Research*, Vol. 40, pp. 1631-1638, 2010.
- [2] Chen, W., Maurel, O., Reess, T., Matallah, M., De Ferron, A., La Borderie, C., Pijaudier-Cabot, G., Rey-Bethbeder, F., Jacques, A. Experimental study on an alternative stimulation technique for tight gas reservoirs based on dynamic shock waves generated by Pulsed Arc Electrohydraulic Discharges. In *J. Petrol. Sci. Eng.*, Vol. 88–89, pp. 67–74, 2012.

- [3] Chen, W., La Borderie, C., Maurel, O., Pijaudier-Cabot, G., Rey-Bethbeder, F., Simulation of damage - permeability coupling for mortar under dynamic loads. In *Int. J. Num. Anal. Meths. in Geomechanics*, Vol. 38, pp. 457-474, 2014.
- [4] Chen, W., Maurel, O., Reess, T., Matallah, M., De Ferron, A., La Borderie, C., Pijaudier-Cabot, G., Rey-Bethbeder, F., Jacques, A. Experimental and numerical study of shock wave propagation in water generated by Pulsed Arc Electrohydraulic Discharges. In *Int. J. Heat and Mass transfer*, Vol. 50, pp. 673-684, 2014.
- [5] Pijaudier-Cabot, G., La Borderie, C., Reess, T., Chen, W., Maurel, O., Rey-Bethbeder, F., de Ferron, A. *Electrohydraulic fracturing of rocks*, ISTE-Wiley Pubs. London, 2016.
- [6] Touya G, Reess T, Pécastaing L, Gibert A, Domens P. Development of subsonic electrical discharges in water and measurements of the associated pressure waves. In *Journal of Physics: Applied Physics*, pp. 5236-5244, 2006.
- [7] Klinkenberg L.J., The permeability of porous media to liquids and gases, American Petroleum Institute. In *Drilling and Production Practice*, pp. 200-213, 1941.
- [8] Madhavan S., Doiphode P.M. and Chaturedi S., Modeling of shock-wave generation in water by electrical discharges. In *IEEE Transactions on Plasma Science*, Vol. 28, pp. 1552-1557, 2005.
- [9] Chatzigeorgiou, G., Picandet, V., Khelidj, A., Pijaudier-Cabot, G. Coupling Between Progressive Damage and Permeability of Concrete: Analysis with a Discrete Model. In *Int. J. Num. Anal. Meths. in Geomechanics*, Vol. 29, pp. 1005-1018, 2005.
- [10] Pijaudier-Cabot, G., Dufour, F. Choinska, M. Permeability due to the increase of damage in concrete: from diffuse to localised damage distributions. In *J. Engrg. Mech. ASCE*, Vol. 135, pp.1022 – 1028, 2009.
- [11] Yuan, S.C., Harrison, J. Numerical modelling of pregressive damage and associated fluid flow using a hydrao-mechanical local degradation approach. In *Int. J. Rock Mechanics & Mining Sciences*, Vol. 41, pp.1-6, 2004.
- [12] Moonen, P., Sluys, L.J., Carmeliet, J., A continuous-discontinuous approach to simulate physical degradation processes in porous media. In *Int. J. Num. Met. Engrg.*, Vol. 84, pp. 1009-1037, 2010.
- [13] Desmorat R, Gatuingt F, Ragueneau F. Nonlocal anisotropic damage model and related computational aspects for quasi-brittle materials. In *Engineering Fracture Mechanics*, Vol. 74, pp.1539-1560, 2007.
- [14] Bažant, Z.P., Jirasek, M., Non local integral formulations for plasticity and damage, survey of progress. In *J. of Engrg. Mech. ASCE*, Vol. 128, pp. 1119-1149, 2002.
- [15] Bary, B., Bournazel, J.P., and Bourdarot E., Poro-Damage Approach Applied to Hydro-Mechanical Fracture Analysis of Concrete. In *J. Engrg. Mech. ASCE*, Vol. 126, pp. 937-943, 2000.
- [16] Schreffler, B., Khoury, G.A., Gawin, D., Majorana, C. Thermo-hydrao-mechanical modelling of high performance concrete at high temperatures. In *Engrg. Comput.*, Vol.19, pp.787-819, 2002.
- [17] Jason L, Pijaudier-Cabot G, Ghavamian S, Huerta A. Hydraulic Behaviour of a Representative Structural Volume for Containment Buildings. In *Nuclear Engineering and Design*, Vol. 237, pp.1259-1274, 2007.
- [18] Robbe M.F., Lepareux M., Cariou Y., Numerical interpretation of the MARA 8 experiment simulating a hypothetical core disruptive accident. In *Nuclear Engineering and Design*, Vol. 220, p.119-158, 2003.
- [19] Robbe M.F., Casadei F., Comparison of various models for the simulation of a Core Disruptive Accident in the MARA 10 mock-up. In *Nuclear Engineering and Design*, Vol. 232, p.301-326, 2004.
- [20] Robbe M.F., Lepareux M., Seinturier E., Computation of a core disruptive accident in the MARS mock-up. In *Nuclear Engineering and Design*, Vol. 235, p.1403-1440, 2005.

- [21] Casadei F., Potapov S., Permanent fluid-structure interaction with non-conforming interfaces in fast transient dynamics. In *Comput. Methods Appl. Mech. Engrg*, Vol.193, p.4157-4194, 2004.